Author(s): Hakala, T. & Puska, Martti J. & Borisov, A. G. & Silkin, V. M. & Zabala, N. & Chulkov, E. V.

Title: Excited states of Na nanoislands on the Cu(111) surface

Year: 2007

Version: Final published version

# Excited states of Na nanoislands on the Cu(111) surface

T. Hakala,[1] M. J. Puska,[1,2] A. G. Borisov,[2,3] V. M. Silkin,[2] N. Zabala,[2,4] and E. V. Chulkov[2,5]
[1]*Laboratory of Physics, Helsinki University of Technology, P.O. Box 1100, FIN-02015 HUT, Finland*
[2]*Donostia International Physics Center (DIPC) and Centro Mixto CSIC-UPV/EHU, Paseo de Manuel Lardizabal, 4, 20018 San Sebastián/Donostia, Basque Country, Spain*
[3]*Laboratoire des Collisions Atomiques et Moléculaires, UMR 8625 CNRS-Université Paris-Sud, 91405 Orsay Cedex, France*
[4]*Elektrizitatea eta Elektronika Saila, Zientzia eta Teknologia Fakultatea, UPV-EHU 644 Posta Kutxa, 48080 Bilbao, Spain*
[5]*Departamento de Física de Materiales, Facultad de Ciencias Químicas, UPV/EHU, Apartado 1072, 20080 San Sebastián/Donostia, Basque Country, Spain*

(Received 12 December 2006; published 27 April 2007)

Electronic states of one monolayer high Na nanoislands on the Cu(111) surface are studied as a function of the nanoisland size. Properties of nanoislands such as one-electron states, the electron density, and the associated potential are obtained self-consistently within the density-functional formalism using a one-dimensional pseudopotential for the Cu(111) substrate and the jellium model for Na. A wave packet propagation method is used to study the energies and lifetimes of quasistationary states localized at Na islands. For very large islands, island-localized states merge into the two-dimensional continuum of the Na quantum well state. Thus, we assign the quasistationary states studied as arising from the quantization of the two-dimensional quantum well continuum due to the finite island size. The scattering at the island boundaries results in the energy-conserving resonant electron transfer into the continuum of the substrate states broadening the island-localized states into resonances.

DOI: 10.1103/PhysRevB.75.165419 PACS number(s): 73.21.Fg, 73.21.La, 73.20.At

## I. INTRODUCTION

Dynamics of excited electrons at surfaces has attracted a lot of experimental and theoretical interest over the last decade.[1–8] This is because of the fundamental and practical importance of these states for surface science. For example, scanning tunneling microscopy and molecular electronics involve electron transfer through the interface, in which surface localized electronic states are of the utmost importance.[9] Moreover, excited electronic states localized on adsorbates often play the role of intermediates in various chemical reactions at surfaces. The lifetimes and decay channels of these states determine the final states of the associated chemical reactions.[10] The recent time-resolved (TR) two-photon photoemission (2PPE) experiments in the femtosecond (fs) time domain[2,3,6,7,11] as well as scanning tunneling spectroscopy (STS) and microscopy measurements[5,7,8,12] have allowed one to probe the electron dynamics in excited states at surfaces and to access such important properties as the characteristic rates for the population and coherence decays.

Long relaxation times for electrons excited to adsorbate-induced electron states have been observed by TR-2PPE on certain noble metal surfaces, e.g., Cu(111), covered by a small amount of alkali metal atoms.[13] On Cu(111), the decay of the adsorbate-localized state to the continuum of bulk metal states via resonant (elastic) one-electron tunneling is efficiently reduced by the energy gap in the projected band structure.[14] In such a situation, the many-body energy relaxation process brings an appreciable contribution to the decay of the excited state.[15] This is an inelastic process involving the interaction between adsorbate-localized and metal electrons. Calculations in which both the elastic and inelastic decay channels are taken into account reproduce the experimentally observed lifetimes of the alkali adsorbate localized states.[15]

When the alkali coverage at the surface increases, excited electronic states localized at individual alkali adsorbate atoms start to overlap and form a quantum well state (QWS), as has been observed by 2PPE, inverse photoemission, and STS for the Na/Cu(111) system.[16–21] Electrons in QWS are confined to the alkali layer by the projected band gap of the substrate and by the vacuum barrier but they move freely parallel to the surface forming a quasi-two-dimensional electron gas. The energy of QWS lowers with increasing alkali coverage. For the monolayer (ML) coverage of Na on Cu(111) the QWS becomes occupied so that the bottom of the QWS band is at −127 meV with respect to the Fermi level. The effective mass $m^*=0.7m_e$ has been measured with STS.[21] Recent *ab initio* calculations of electronic properties of the $(2\times2)$ and $(3/2\times3/2)$ adsorbate structures for Na/Cu(111) (Ref. 22) report on results in close agreement with the STS data. Lifetimes of holes in quantum well states at surface overlayers have been measured with STS (Ref. 23) and photoemission spectroscopy.[19] The inelastic electron-electron scattering contribution to the hole lifetime together with the contribution of the electron-phonon scattering has been calculated for 0.95 and 1 ML of Na on the Cu(111) surface.[23] According to both experiment and theory the hole lifetimes decrease nearly by a factor of 2 when the coverage increases from 0.95 to 1 ML. This is explained by the increase of the phase space for the intraband electron-electron scattering processes within the QWS band. With detailed experimental and theoretical studies of Na/Cu(111) with different coverages of Na, this system plays the role of the prototype system for studying electron dynamics for various adsorbate/substrate combinations.[24,25]

Along with formation of overlayer structures, controlled growth of epitaxial layers can result in the formation of small islands.[26] Thus, Ag islands of 1 ML in height are formed

 

during epitaxial growth on Ag(111) at room temperature.[27] Na islands are formed in the second ML of Na on the Cu(111) surface,[17,20,21] but it is argued that hexagonal-shaped Na islands could be formed in the first ML on top of the close-packed (111) surface.[28] Also, the apparent discontinuity in the properties of QWS observed at a certain coverage range (0.4 ML) has been tentatively attributed to the island formation.[18] Nanoislands are the two-dimensional (2D) analogs of the supported metal clusters.[29] The latter represent an important research subject *per se* because of their role in catalysis.[30] From the fundamental point of view, electronic states localized in clusters couple to the continuum of electronic states of the metallic substrate, and so they are broadened into resonances naturally raising the question about their lifetimes.

In order to understand surface reactions at adatom islands and also to get a systematic physical picture it is important to study how the electronic structure develops as the island size increases. The first studies of electronic properties of Na islands (metallic quantum dots) supported on Cu(111) substrate have been reported for Na islands formed in the second monolayer on top of the 1ML Na/Cu(111) system.[31] Both the Cu substrate and the Na adsorbate were treated in density functional theory (DFT) within the free-electron metal (jellium) approximation. Results have been obtained regarding electronic states and reactivity of the supported nanoscale system. However, the effect of the projected band gap of the Cu(111) band structure, known to result in stabilization of the adsorbate-localized states,[15] cannot properly be accounted for within the jellium model.

The purpose of the present work is to study the effect of the projected band gap on the properties (energies and widths) of electronic states localized in supported metal nanoislands and create a systematic picture of the variation of these properties with the island size. 1 ML high Na islands on Cu(111) are addressed here as the prototype system. The reason for this choice is that the single adatom and complete monolayer cases are well documented in the literature providing the basis for the size-variation studies. In particular, we are interested in how the dynamics of QWS is influenced by the finite island size. Indeed, scattering of 2D QWS electrons at island boundaries leads to a quantization effect with emerging of discrete island-localized states. On the other hand, scattering events open the possibility for energy-conserving resonant electron transfer into the three-dimensional (3D) continuum of the bulk states so that the island-localized states are broadened into resonances. One can note that similar to QWS, surface states at the (111) surfaces of noble metals form a 2D electronic continuum with quasifree electron motion parallel to the surface. In this respect the systems studied here have a direct link to the quantization of the 2D surface state continuum observed, e.g., at quantum corrals[32,33] as well as at Ag adatom[27] or vacancy[34] islands on the Ag(111) surface.

We solve for the self-consistent electronic structures of Na adatom islands on the Cu(111) within the DFT.[35] The Cu(111) substrate is described by a one-dimensional pseudopotential[36,37] varying perpendicular to the surface and the Na islands are treated by the jellium model in the cylindrical geometry. The islands considered contain up to 61 Na atoms and in the ground state they exhibit unoccupied quasistationary single-electron states. We calculate the lifetimes of electrons excited to these resonant states. The elastic one-electron tunneling contribution to the decay is calculated by the wave packet propagation (WPP) method.[15] The many-electron inelastic contribution is estimated from the *GW* approximation results for QWS's at 1ML of Na on the Cu(111) surface.[38]

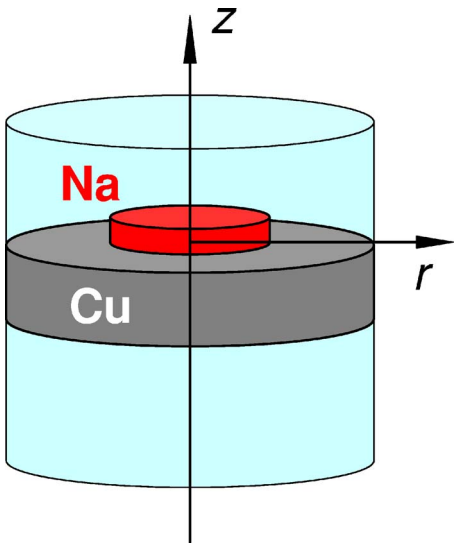


FIG. 1. (Color online) Schematic presentation of the cylindrical calculation volume with a Na nanoisland on the top of the Cu(111) surface. The $z$ and $r$ axis of the cylindrical coordinates are also shown.

The organization of the present paper is as follows. In Sec. II we briefly describe the theoretical models used and their implementation. Section III contains our results and discussion and Sec. IV is a short summary. Atomic units with $\hbar = e^2 = m_e = 1$ are used throughout the equations of the paper. The atomic unit (a.u.) of the length used is the Bohr radius $a_0$.

## II. METHODS

### A. Self-consistent electronic-structure calculations

Even though the Kohn-Sham orbitals have no direct meaning in the DFT when it comes to describing electron states above the Fermi level, they are usually a good starting point for describing the real quasiparticles within many-body perturbation formalism.[35] Our first task is thus to obtain the self-consistent electronic structures of Na nanoislands on the Cu(111) surface using the DFT within the local-density approximation (LDA).[39] In the present study, the cylindrically symmetric Kohn-Sham equations are solved in real space using multigrid techniques.[40,41]

Figure 1 shows schematically our model for Na nanoislands on the Cu(111) surface. Inside the Cu slab the electron-ion interaction is simplified using a one-dimensional pseudopotential constructed[36] on the basis of the corresponding model potential.[37] The model potential[37] is only a function of the electron-surface distance along the surface normal. It re-

produces the main physical features of the Cu(111) surface at the $\bar{\Gamma}$ point: The projected band gap between −5.83 and −0.69 eV (all energies are measured with respect to the vacuum level), the Shockley-type surface state at −5.33 eV, and the first image potential state at −0.82 eV. In the self-consistent calculations the neutralizing rigid positive background charge, being equal to the average electron density within the Cu slab, corresponds to the density parameter $r_s^{\mathrm{Cu}}=(3n_{\mathrm{Cu}}/4\pi)^{1/3}=2.55$ a.u. This is close to the experimental value of 2.67 a.u. for Cu 4*s* electrons. By construction of the pseudopotential,[36] the self-consistent LDA electronic structure of the clean Cu(111) reproduces the results of the model potential and the correct experimental position of the Fermi level, i.e., −4.94 eV with respect to the vacuum level. The Cu slab has 21 Cu(111) layers corresponding to the thickness of 83 a.u. The slab has to be thick enough to minimize the interaction between the two surfaces. However, the thickness is limited by the fact that the calculation volume has to be large also in the lateral direction and a compromise has to be sought to keep the calculations feasible. Our calculations are restricted to a cylinder of radius $R=40$ a.u. and a height of 156 a.u. (the boundary conditions are explained below). Thus, approximately 6000 electrons in the Cu slab have to be treated self-consistently which is a challenge in parallel computing.

Hexagonal-shaped Na clusters are observed to be formed on top of close-packed (111) surfaces.[28] In our model the hexagonal Na clusters are substituted by cylinders of rigid jellium background charge as shown in Fig. 1. We also ignore the possible island-size-dependent relaxation of the atoms at the island edges.[42] Because the length scale of confinement-related electron density variation at the island edge is larger than the atomic relaxations the ensuing effect on the overall behavior of the electronic structure is expected to be minor. Thus, despite its simplicity the jellium cylinder model is expected to give a meaningful description of the actual hexagonal Na clusters with free-electron character in terms of the trends predicted. We use the jellium background density with $r_s^{\mathrm{Na}}=3.93$ a.u. corresponding to bulk Na. The height of the nanoislands is that of a single monolayer 5.5 a.u. as obtained in STM measurements.[21] We also calculate the electronic structure for 1ML Na/Cu(111) and the bottom of the ensuing QWS band is adjusted to its experimental value of −0.127 eV with respect to the Fermi level[21] by varying the distance between the Na layer and the Cu surface. The resulting distance $Z_{\mathrm{Na}}=4.46$ a.u. between the topmost Cu layer and the midpoint of the Na layer means a slight overlap of the positive background charges. This distance is then also used for the Na islands. Islands with 1, 3, 7, 19, 37, or 61 Na atoms are considered; the four largest ones corresponding to completed hexagonal islands.

With the *z* axis chosen perpendicular to the surface and going through the center of the island, the potential of the system is cylindrically symmetric. The Schrödinger equation is separable in cylindrical coordinates, and the Kohn-Sham orbitals have the form

$$U_{mGl}(\mathbf{r})=\frac{1}{\sqrt{2\pi}}e^{im\varphi}u_{mGl}(r,z). \quad (1)$$

Above, *r* is the radial variable in a plane parallel to the surface, *m* is the azimuthal quantum number, and *G* refers to boundary conditions at the maximum radius of calculations, i.e., to the $\mathbf{k}_\parallel$-point sampling discussed below. Moreover, *l* differentiates between orthogonal states with the same *m* and *G*. This form of wave function has two important features. First, for a given three-dimensional problem, only a two-dimensional numerical solution is required as the angular part is analytic. Second, wave functions with different quantum numbers *m* and *G* are automatically orthogonal allowing easy parallelization in modern parallel computing environments. Therefore it is possible to self-consistently solve systems consisting of thousands of electrons.

In our real-space calculations wave functions, densities, and potentials are given on a uniform grid of $127\times316$ points, in *r* and *z* directions, respectively. When solving for the Poisson equation, the computational cell is extended to 120 a.u. in the *r* direction by adding charge of the clean surface and to 2340 a.u. in the *z* direction by adding vacuum. Thereby the slowly decaying dipole component of the Coulomb potential is described accurately enough.

The boundary conditions for the wave functions are defined as follows. The wave functions are required to vanish above and below the Cu/Na slab at the top and the bottom of the cylindrical calculation volume. On the cylindrical boundary we employ two different conditions. Namely, either the wave function itself or its derivative $\partial u_{mGl}/\partial r$ is set to zero. The first case corresponds in the Wigner-Seitz (super)cell approximation[43] to a wave vector at the Brillouin zone boundary and we label the wave functions with $G=L$ in analogy with usual band-structure calculations. The second case corresponds to a wave vector at the Brillouin zone origin and thus the label $G=\Gamma$. The energy eigenvalues of the *L* and Γ states correspond to the tops and bottoms of certain energy bands in the (super)lattice, respectively. The use of the two different boundary conditions $G=\Gamma,L$ results in a radially constant charge density far from defects (see Fig. 2) and a free-electron-like band structure as a function of the momentum $k_\parallel$ parallel to the surface (Fig. 3). Our calculations demonstrate clearly the advantage of real-space methods in handling different types of boundary conditions for the potential and the wave functions.

In order to illustrate the sampling of different eigenstates we show in Fig. 3 the $m=0$ eigenenergies for the clean Cu(111) surface in the energy range from −9 to −3 eV. The energy zero corresponds to the vacuum level. The energies are given as a function of the momentum $k_\parallel$ parallel to the surface. The $k_\parallel$ values are obtained as follows. The number of vertical nodes *l* is first counted by inspecting the behavior of the given wave function along the radial axis between $r=0$ and the maximum radius $r=R$. For the Γ states $k_\parallel=y_l/R$, where $y_l$ is the *l*th zero of the derivative of the zeroth-order Bessel function $J_0(x)$ (the zero at $x=0$ is excluded). For the *L* states $k_\parallel=x_l/R$, where $x_l$ is the *l*th zero of $J_0(x)$. As shown in Fig. 3 the eigenenergies form the surface state band and the region of projected bulk bands. Both the surface and bulk state eigenenergies fall on parabolas corresponding to free electron motion parallel to the surface and the effective mass of unity. This is consistent with our choice of the model potential that depends only on the *z* coordinate. The eigenenergies of the $m>0$ states fall on slightly different $k_\parallel$ values but on the same parabola as those of the $m=0$ states. Thus,

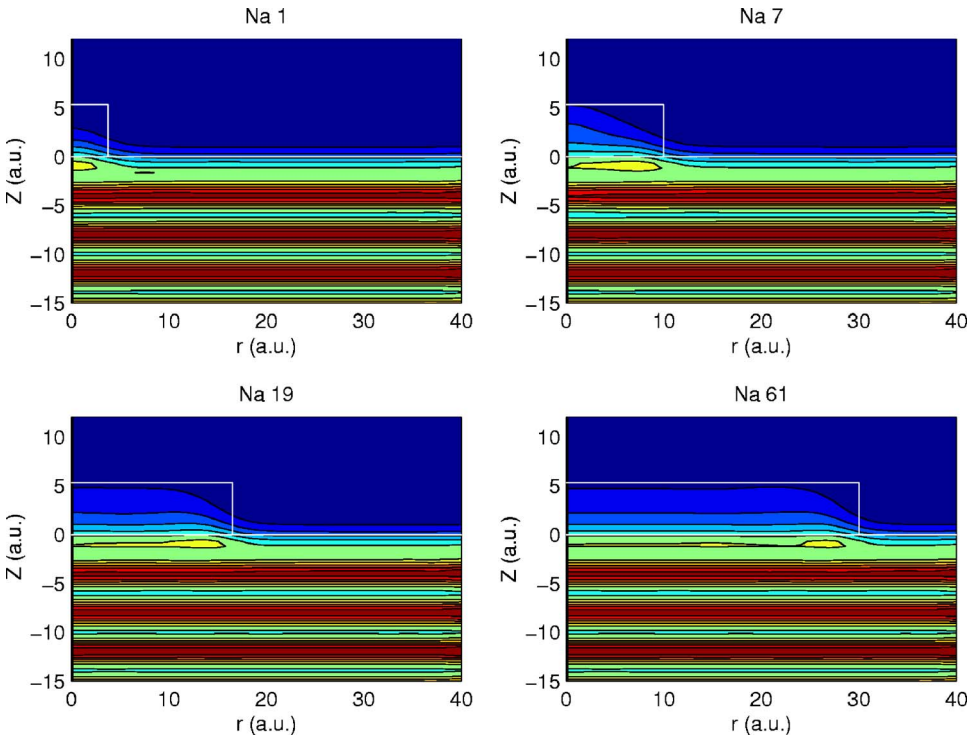


FIG. 2. (Color online) Electron densities for Na nanoislands on the Cu(111) surface. The islands comprise 1, 7, 19, and 61 Na atoms. The white lines show the Cu(111) surface and the Na cluster on top of it by giving the edges of the positive background charges. $z=0$ corresponds to the position of the image plane of Cu(111) (Ref. 37), and inside the metal $z$ is negative. The electron density decreases when going from red to violet.

the real sampling of states is denser along the $k_{\parallel}$ axis than that shown in Fig. 3. The finite energy gaps between adjacent bulk state parabolas reflect the vertical confinement inside the Cu slab.

The self-consistency of our electronic structure calculations means a step from more empirical modeling towards first-principles calculations. On the other hand, the remaining simplicity of our modeling, i.e., the jellium model for the adsorbate and the translational invariance of the substrate along the surface still conserves the essential physical ingredients such as the projected band gap along the (111) direction in Cu and gives physical insight as transparent trends.

### B. Calculation of the energies and lifetimes of the island-localized states

The large number of electronic states involved in our DFT study makes recognition of the island-localized states difficult, especially in the case of weak localization. Moreover, the broadening of these states into resonances and the discrete sampling of the continuous energy spectrum means that several discrete states may correspond to the same resonant state. Therefore, within this DFT framework extraction of the resonance characteristics is not a trivial task and we will rely on the WPP approach in extracting the energies, decay rates, and wave functions of the island-localized resonances. The self-consistent DFT calculations provide the inputs for the WPP calculations.

Since the detailed overview of the WPP method has been given elsewhere,[15,44,45] we only outline here the basic principles related to the present work. The core of the WPP method consists of the direct solution of the time-dependent Schrödinger equation for the wave function of the "active" electron. In the present case the system possesses cylindrical symmetry with respect to the $z$ axis and the obvious choice of the wave function representation is

$$\Psi(r,\varphi,z,t) = \sum_m \frac{1}{\sqrt{2\pi}} e^{im\varphi} \psi_m(r,z,t). \tag{2}$$

A discrete mesh in $(r,z)$ spatial coordinates is used. The components $\psi_m(\rho,z,t)$ evolve in time independently according to

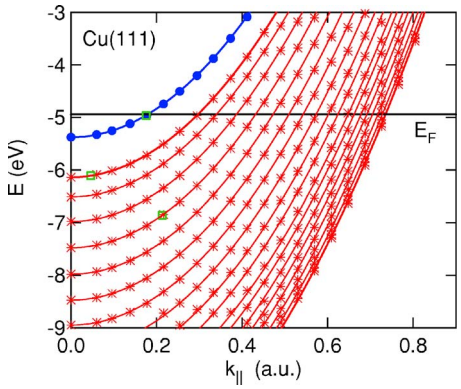


FIG. 3. (Color online) Electronic structure of the clean Cu(111) surface system according to our DFT calculations. The filled circles and stars denote $m=0$ energy eigenvalues and correspond to the surface and bulk states, respectively. Few $m=1$ eigenvalues are given by open green squares. The identification of the parallel momentum values is explained in the text. The solid lines correspond to the parabolic free-electron dispersion with unit effective mass. The thick red lines bracket the projected bulk bands and the blue line is the surface state band. The black horizontal line denotes the Fermi level.

$$i\frac{\partial\psi_m(r,z,t)}{\partial t} = H_m\psi_m(r,z,t). \tag{3}$$

$H_m$ stands for the effective Hamiltonian responsible for the time evolution within the $m$th subspace, i.e.,

$$H_m = -\underbrace{\frac{1}{2}\frac{\partial^2}{\partial z^2}}_{\hat{T}_z} - \underbrace{\frac{1}{2r}\frac{\partial}{\partial r}r\frac{\partial}{\partial r}}_{\hat{T}_r} + \frac{m^2}{2r^2} + V(r,z). \tag{4}$$

Potential $V(r,z)$ is constructed along the lines of previous studies of adatom induced states in the Cu/Cu(111) and Cu/Cu(100) systems[46] as

$$V(r,z) = V_s(z) + V_{\mathrm{Na}}(r,z) + V_{\mathrm{opt}}(r,z), \tag{5}$$

where $V_s(z)$ is the above-discussed model potential describing the Cu(111) surface.[37] Importantly, $V_s(z)$ represents the semi-infinite Cu(111) surface in our WPP study, and not a Cu(111) slab. The second term corresponds to the island-induced potential given by two terms as $V_{\mathrm{Na}}(r,z) = \Delta V_{\mathrm{XC}}(r,z) + \Delta V_H(r,z)$. Here, the induced exchange-correlation potential $\Delta V_{\mathrm{XC}}$ is obtained as a difference between the DFT potential for the complete system of the Na island and the Cu(111) slab and the potential of the bare Cu(111) slab, i.e., $\Delta V_{\mathrm{XC}}(r,z) = V_{\mathrm{XC}}^{\mathrm{Na+Cu(111)}}(r,z) - V_{\mathrm{XC}}^{\mathrm{Cu(111)}}(r,z)$. The induced Hartree potential $\Delta V_H$ is calculated on the WPP mesh by the direct solution of the Poisson equation with the DFT island-induced charge density as the source term. We have chosen this potential construction instead of the direct input of the DFT potential for the complete system. The reason is twofold. (i) The Cu(111) slab geometry used in the DFT study would necessarily lead to the undesired quantization of the continuum of the electronic states of the substrate. (ii) Owing to the spatial localization of the $\Delta V_{\mathrm{XC}}(r,z)$, and the island-induced charge density one can easily obtain the potential on the WPP mesh with the flexibility of choosing the grid for the spatial coordinates. In fact, the wave packet propagation is performed in a much larger computation volume than the self-consistent electronic structure calculations. Clearly, comparing the energies of the island-localized states as obtained with the two methods (DFT and WPP) is the first check for the consistency of our calculations. Typically, when the identification of the corresponding eigenstates of the DFT and WPP calculations is clear the eigenenergies agree within the accuracy of around 0.1 eV.

Finally, $V_{\mathrm{opt}}(r,z)$ is the optical absorbing potential[47] introduced at the boundaries of the mesh in order to suppress artificial reflections of the wave packet. It imposes the outgoing wave boundary conditions consistent with the search of the quasistationary states. Thereby, in the WPP we completely avoid the finite-size effects.

The time dependent solution $\psi_m(r,z,t)$ of Eq. (3) with the Hamiltonian given by Eq. (4) is obtained numerically with the split operator technique[48]

$$\psi_m(r,z,t+\Delta t) = e^{-i(\Delta t/2)V}e^{-i\Delta t T_z}e^{-i\Delta t T_r}e^{-i(\Delta t/2)V}\psi_m(r,z,t) + O(\Delta t^3). \tag{6}$$

The Fourier-grid pseudospectral approach[49] is used to calculate the action of the $e^{-i\Delta t T_z}$ operator and the Cayley transform technique[50] with three-point finite differences is used to calculate the action of the $e^{-i\Delta t T_r}$ operator. For further details, see Ref. 44. The initial conditions $\psi_m(r,z,t=0)$ are defined in each $m$ subspace of interest. In practice, we use Gaussian-shape wave functions chosen in such a way that they have the largest possible overlap with the quasistationary states localized on the Na island. Thus,

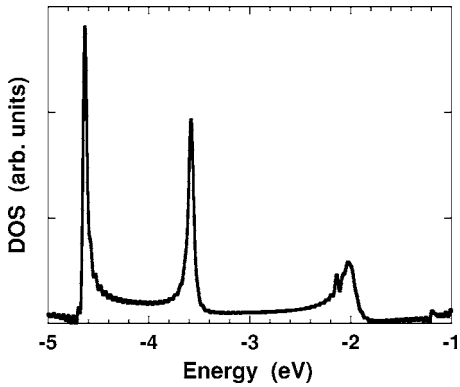


FIG. 4. Projected density of the $m=0$ symmetry states as function of the energy. The WPP results are shown for the nanoisland comprising 19 Na atoms. The energy is referred to the vacuum level.

$$\psi_m(r,z,t=0) = r^m e^{-\alpha(z-Z_{\mathrm{Na}})^2}\{e^{-\beta(r-R_{\mathrm{Na}})^2} + e^{-\beta r^2}\}, \tag{7}$$

where $\alpha$ and $\beta$ are parameters and $R_{\mathrm{Na}}$ is the radius of the Na island. Once the $\psi_m(r,z,t)$ solution is obtained it is analyzed to extract the physical quantities of interest. Thus, the Laplace transform of the survival amplitude $A_m(t) = \langle\psi_m(r,z,t=0)|\psi_m(r,z,t)\rangle$ provides the density of states (DOS) projected on the initial state

$$\sigma_m(E) = \frac{1}{\pi}\mathrm{Re}\left\{\int_0^\infty dt e^{i(E+i\eta)t}A_m(t)\right\}, \tag{8}$$

where $E$ is the energy and the small real constant $\eta \to +0$. In practice, $\eta$ is set to 0 because its role is played by the absorbing potential $V_{\mathrm{opt}}$. We give in Fig. 4 an example of the projected density of states $\sigma_0(E)$ calculated for the nanoisland comprising 19 Na atoms. The energies and widths of the quasistationary electronic states localized at the island can be obtained from the energy positions and widths of the corresponding peaks in the DOS. However, oscillating structures as well as additional broadening of the peaks arise because, in practice, the integration in Eq. (8) is truncated at a finite maximum time. This also means that the resonances are relatively long-lived and prohibitively long propagation times would be needed for convergence. This problem is avoided via a direct fit of the $A(t)$ signal to a sum of exponentially decaying terms

$$A_m(t) = \sum_{j=0}^{J} a_j e^{-i[E_{mj} - i(\Gamma_{mj}/2)]t}. \tag{9}$$

Some parameters are stable with respect to the truncation of the sum at $J$. They are associated with the energies $E_{mn}$ and

the widths $\Gamma_{mn}$ of the resonances. The procedure defined by Eq. (9) works well if the number of resonances contributing to $A(t)$ is small. For cases with large numbers of resonances the "filter diagonalization" technique[51–53] is preferred.

The wave function of the quasistationary (resonance) state at the energy $E_{mn}$ is obtained from the time-dependent solution $\psi_m(r,z,t)$ as

$$\psi_m^{\mathrm{res}}(r,z,E_{mn}) = \int_0^\infty e^{iE_{mn}t}\psi_m(r,z,t)dt. \tag{10}$$

The extracted $\psi_m^{\mathrm{res}}(r,z,E_{mn})$ serves for the assignment of the states and for an additional check of the consistency of the $E_{mn}$ ($\Gamma_{mn}$) extraction. Indeed, if it is used as the initial state in the WPP procedure, the corresponding autocorrelation function can be represented by a single exponential term in Eq. (9).

## III. RESULTS AND DISCUSSION

In order to relate the present study to the earlier study of Ref. 15 for the energy and lifetime of the excited state localized at single Na adsorbate on Cu(111), we have calculated the smallest cylindrical Na island corresponding to 1 Na atom. The island-localized resonance state has the $m=0$ symmetry. The energy is found to be −2.11 eV with respect to the vacuum level and the width $\Gamma_{00}=143$ meV, corresponding to the lifetime $\tau_{00}=1/\Gamma_{00}=4.6$ fs. The energy obtained is close to −2.17 eV found in the earlier study,[15] where the Na-ion pseudopotential was used to represent the Na adsorbate. Regarding the resonant electron transfer rate into the metal, given by $\Gamma_{m=0\ n=0}$, the present result is twice the earlier one. Overall, the present cylindrical jellium approximation appears quite reasonable despite its simplicity. The difference in the widths can be attributed to the difficulty to properly represent the *s-p* hybridization within the "cylindrical" atom model. Primarily, this is an obvious consequence of the present cylindrical shape of the Na adsorbate, while the latter should correspond to the spherical symmetry as automatically taken into account with ionic pseudopotential. Secondly, the ionic pseudopotential is adjusted to energy spectrum of the gas-phase Na atom (in particular the $3s$-$3p$ energy difference determining the *s-p* hybridization is exactly reproduced). The jellium model of the single Na atom with LDA treatment of the exchange-correlation kernel does not yield the exact energy separation between atomic orbitals. The *s-p* hybridization pushes the electronic density of the adsorbate-localized state out from the surface. It thus reduces the coupling between the adsorbate-localized state and continuum of substrate electronic states leading to the small electron transfer rates in front of surfaces with projected band gaps.[15]

Prior to discussing the results obtained for the Na nanoislands let us first introduce a simple model. As has been discussed in the preceding sections, QWS is formed for the complete Na monolayer on Cu(111) surface. In the direction of the surface normal the electron in QWS is confined to the Na monolayer. It is bound between the Na/vacuum and Na/Cu(111) interfaces because of the projected $L$ band gap of the Cu(111)-substrate. In the direction parallel to the surface, the QWS electron moves quasifreely so that the 2D continuum of electronic states is formed. Within this model, in which the potential depends only on the $z$ coordinate being perpendicular to the surface, the wave function of QWS is given by $\psi_{\mathbf{k}_\parallel}^{\mathrm{QW}}(\mathbf{r},z)=f^{\mathrm{QW}}(z)\exp\{i\mathbf{k}_\parallel\mathbf{r}\}$, where $\mathbf{k}_\parallel$ is the wave vector in a direction parallel to the surface and $f^{\mathrm{QW}}(z)$ is a bound state wave function corresponding to the energy $E_{\mathrm{QW}}=-0.127$ eV (bottom of the QWS band) with respect to the Fermi level. The energy dispersion of the $\psi_{\mathbf{k}_\parallel}^{\mathrm{QW}}$ states is given by the free electron parabola $E(\mathbf{k}_\parallel)=E_{\mathrm{QW}}+k_\parallel^2/2$. Aside from the possible band-folding effects,[54] 1 ML Na QWS's are stable within the one-electron picture. The many-body decay of QWS's proceeds via electron-electron and electron-phonon scattering.[23]

Consider now that instead of the complete Na monolayer we deal with a large cylindrical Na island. The QWS electron moving inside the Na island will be reflected by the island boundaries, so that discrete states will emerge instead of the 2D continuum of states. Under the assumption of a complete reflection at $r=R_{\mathrm{Na}}$, the wave functions of the discrete states are given by

$$\psi_{mn}(r,\varphi,z) = f^{\mathrm{QW}}(z)J_m(k_{mn}r)e^{im\varphi}, \tag{11}$$

where the states are characterized by two quantum numbers $m$ and $n$. For the $n$th state within $m$-symmetry subspace, the wave vector value is given by $k_{mn}=R_{mn+1}/R_{\mathrm{Na}}$, where $R_{mn+1}$ is the $(n+1)$th zero of the Bessel function $J_m(x)$ (different than $x=0$ for $m\neq 0$). The quantum number $n$ runs over the $(0,1,2,\ldots)$ sequence and corresponds to the number of nodes of the wave function in the $r$ direction inside the island. (Actually, we use this procedure with the radius of the cylindrical calculation volume above to determine the wave vectors $k_\parallel$ of the clean surface $G=L$ states of our DFT calculations.) The confinement lifts the $m$ degeneracy of the 2D continuum states and the energies of the "particle-in-a-box" states can be found from

$$E_{mn} = E_{\mathrm{QW}} + k_{mn}^2/2 = E_{\mathrm{QW}} + (R_{mn+1}/R_{\mathrm{Na}})^2/2. \tag{12}$$

If the reflection at the island boundaries is not complete, one-electron energy-conserving decay channels open. These correspond to the electron scattering into substrate states. The island-localized states broaden into resonances. In what follows we show that this intuitive picture appears to explain the results of the complete calculation.

The systems studied are summarized in Table I. We have concentrated only on the states converging to QWS in the limit of the large island size. The localization of the image potential states[55] and related issues are beyond the scope of the present study. The classification of the states can be directly performed from their shape in the $z$ direction and their nodal structure in the $r$ direction as revealed by the densities $|\psi_m^{\mathrm{res}}(r,z,E_{mn})|^2$ (see below). The island-localized resonances are extracted in the energy range from −5 to −1.5 eV with respect to the vacuum level. The spin and the $\pm m$ degeneracies are not accounted for in Table I. For example, the degenerate $\pm m$ states are counted as one state.

TABLE I. Island size dependence of the number of island-localized states ($N_{st}$) found in the energy interval from −5 to −1.5 eV with respect to the vacuum level. The results are symmetry resolved ($m$ quantum number). $N_{Na}$ is the number of the Na atoms in the island. $R_{Na}$ is the radius of the corresponding jellium cylinder (the radius of the rigid positive background charge).

| | | $\|m\|$ | | | | | | | | | | |
|---|---|---|---|---|---|---|---|---|---|---|---|---|
| $N_{Na}$ | $R_{Na}$ | 0 | 1 | 2 | 3 | 4 | 5 | 6 | 7 | 8 | 9 | $N_{st}$ |
| 1 | 3.84 | 1 | | | | | | | | | | 1 |
| 3 | 6.64 | 1 | 1 | | | | | | | | | 2 |
| 7 | 10.15 | 2 | 1 | 1 | 1 | | | | | | | 5 |
| 19 | 16.72 | 3 | 3 | 2 | 1 | 1 | 1 | | | | | 11 |
| 37 | 23.33 | 4 | 3 | 3 | 2 | 2 | 2 | 1 | 1 | | | 18 |
| 61 | 29.96 | 5 | 5 | 4 | 4 | 3 | 3 | 3 | 2 | 2 | 1 | 32 |

As a general trend seen in Table I, the number of island-localized states increases with the increasing island size. This concerns both (i) the number of the states within a given $m$ symmetry and (ii) the number of $m$ subspaces, where island-localized states are found. For example, for the nanoisland of 7 Na atoms 5 states are found with the maximum value of $m=3$ and for the island of 37 Na atoms 18 states are found with maximum value of $m=7$.

Electron densities of island-localized, $m=0$ symmetry quasistationary states are shown in Fig. 5 for the case of the nanoisland comprising 61 Na atoms. Logarithmic scale is used. For the sake of comparison with the particle-in-a-box picture we classify the states according to the $(m,n)$ pair of the quantum numbers. As follows from present results, the $(m=0,n=0)$ wave function corresponding to the lowest energy eigenvalue spreads over the entire nanoisland in the $r$ direction. The main peak in the $z$ dependence of the electron density is located at the Na island, whereas damped oscillations along the $z$ axis inside the metal correspond to the decaying exponent behavior due to the band gap. Based on the shapes of the wave functions we argue that the observed states correspond to the Na QWS localization at the island. To prove this statement, we compare in Fig. 6 the $z$ dependence of the electron density of QWS for 1ML Na on Cu(111) and that of the $(m=0,n=0)$ island-localized state. The former is given by $|f^{QW}(z)|^2$, and the latter is taken in the middle of the island: $|\psi^{res}_{m=0}(r=0,z,E_{00})|^2$. The $f^{QW}(z)$ wave function is calculated using the effective DFT potential of the 1ML Na/Cu(111) system. We see that the $z$ behavior of the island-localized state indeed coincides with that of QWS.

The assignment of the origin of the calculated states as Na 2D QWS continuum confined by the island is further supported by the shape of the wave functions of the higher energy states within the $m=0$ symmetry subspace. The nodal structure develops in the $r$ direction. The $(m=0,n)$states show $n$ nodes in complete accord with the prediction of Eq. (11). The wave functions of the quasistationary states associated with the $m\neq 0$ subspaces are also consistent with the particle-in-a-box picture.

Up to now we have only discussed the quantization aspect. As shown schematically in Fig. 7, an island-localized state is in resonance with 3D continuum states within the range of finite $k_{\|}$ values, as well as with a given $k_{\|}$ state of the 2D surface state continuum. (The bottom of the surface state band is located at approximately −5.3 eV with respect to the vacuum level.) Since the island boundaries are not perfectly reflective, the island-localized states can decay via energy conserving resonant electron transfer into the surface state continuum or into the 3D bulk continuum. Therefore the confined states become quasistationary, i.e., they are broadened into resonances.

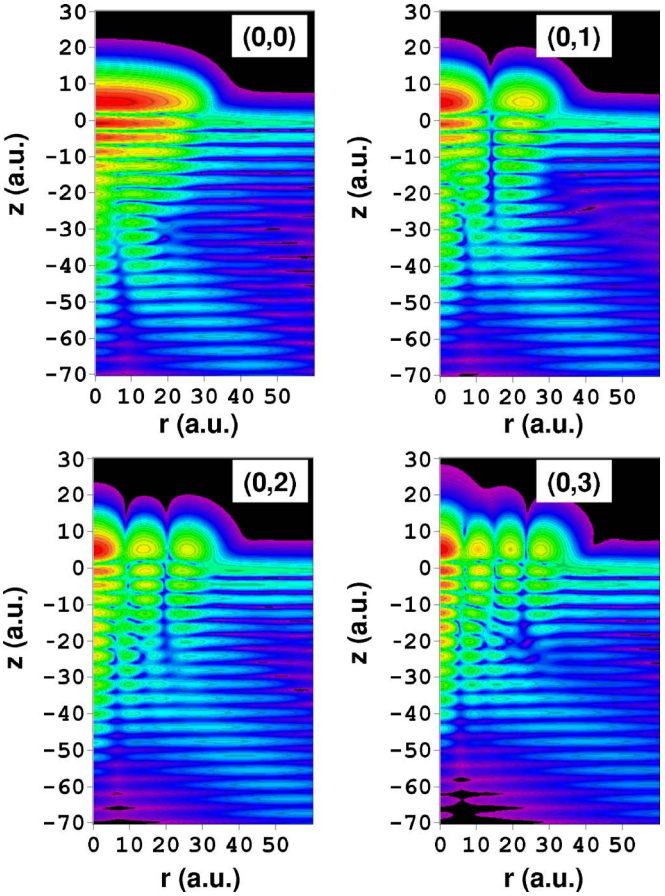


FIG. 5. (Color online) Interpolated images of the electron density of the $(m=0,\ n=0,1,2,3)$ quasistationary island-localized states for the 61 Na atom island on the Cu(111) surface. The logarithm of the density $\ln\{|\psi^{res}_{m}(r,z,E_{mn})|^2\}$ is shown in cylindrical coordinates, parallel ($r$) and perpendicular ($z$) to the surface. $z=0$ corresponds to the position of the image plane of the Cu(111) surface (Ref. 37), and inside the metal $z$ is negative. The electron density decreases from 1 to 0.001 (arbitrary units) when going from red to violet. The states are labeled according to their quantum numbers, as explained in the text.

The decay into the surface state continuum is clearly visible in Fig. 5 as the outgoing flux of electrons in a direction parallel to the surface. As for the decay into the 3D bulk continuum, it is blocked in the direction of the surface normal because of the projected band gap. It appears then as the outgoing flux at a finite angle with respect to the $z$ axis, corresponding to the population of continuum states with a finite $k_{\|}$ (see Fig. 7). Qualitatively, these features are similar to earlier results obtained for alkali adsorbate atoms.[14,15]

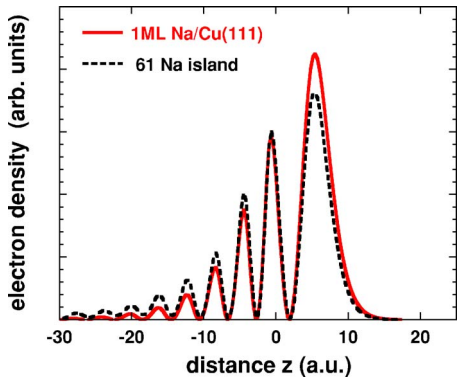


FIG. 6. (Color online) Comparison of the electron density of QWS's for 1ML Na on the Cu(111) surface and that of the $(m=0, n=0)$ quasistationary state at the 61 Na atom island. The density is shown as a function of the electron coordinate perpendicular to the surface $z$. For the island-localized state the $z$ dependence of the density corresponds to the middle of the island, i.e., it is given by $|\psi^{\mathrm{res}}_{m=0}(r=0,z,E_{00})|^2$. The normalization of the two densities is arbitrary. $z=0$ corresponds to the position of the image plane of the Cu(111) surface (Ref. 37), and inside the metal $z$ is negative.

The calculated energies of various $(m,n)$ quasistationary states of the 61 Na atom nanoisland are shown Fig. 8. The energy is presented with respect to the vacuum level as a function of $(k_{mn})^2/2$. Consistent with the prediction of Eq. (12) the results fall on a straight line. Thus, for the largest island studied here, we clearly observe that island-localized states result from the particle-in-a-box quantization of the 2D QWS continuum. A slight deviation from the straight-line behavior can be observed for the high-$n$ (low binding energy) states. It is attributed to the large spatial extension of the wave function in the $r$ direction outside the island boundaries, the latter being not perfectly reflecting. This necessarily lowers the energy of the state as compared to the one estimated from the zero boundary conditions at $R_{\mathrm{Na}}$.

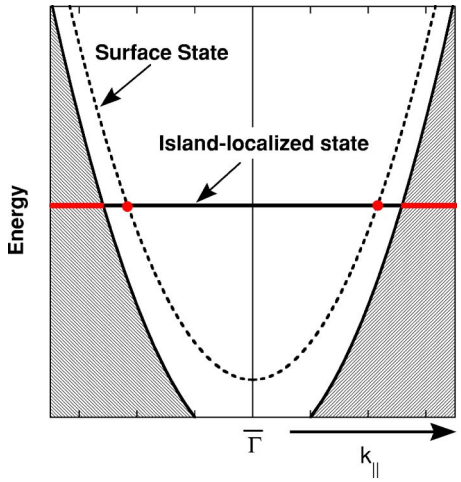


FIG. 7. (Color online) Cu(111) substrate states available for the one-electron energy conserving transitions from the Na island-localized state. The states contributing to the decay of the quasistationary state are shown by red filled circles (surface state) and red lines (bulk states). The figure shows the energies of the states as a function of the electron momentum parallel to the surface $k_{\parallel}$. The black horizontal line corresponds to the island-localized state.

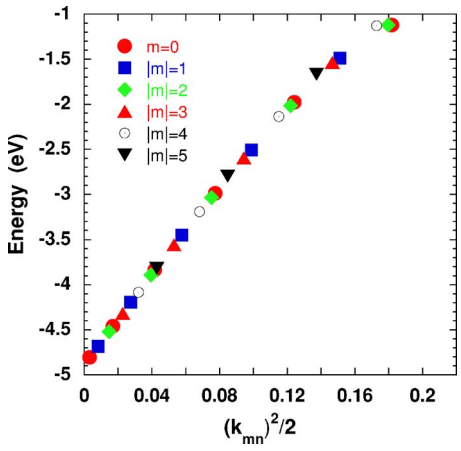


FIG. 8. (Color online) Energy of various $(m,n)$ quasistationary states of 61 Na atom nanoisland on Cu(111). The energy is referred to the vacuum level. The results are shown as a function of the quantized wave vector of the corresponding particle-in-a-box states (see the text for the definition). The different symbols represent states of the different $m$ symmetries, as shown in the inset.

Figure 9 summarizes the results obtained for the energy of the island-localized states for islands of sizes ranging from 1 to 61 Na atoms. For a given island size, the states corresponding to different $m$ symmetries are represented by the same symbol. The results are shown as a function of $(k_{mn})^2/2$. Obviously, starting from the 19 Na atom nanoisland, the particle-in-a-box model for the QWS trapped in the island works extremely well. For the smaller islands, the weight of the exponential tails of the wave functions outside the island boundary $R_{\mathrm{Na}}$ becomes more and more important. Therefore, the simple model expressed by Eq. (12) cannot

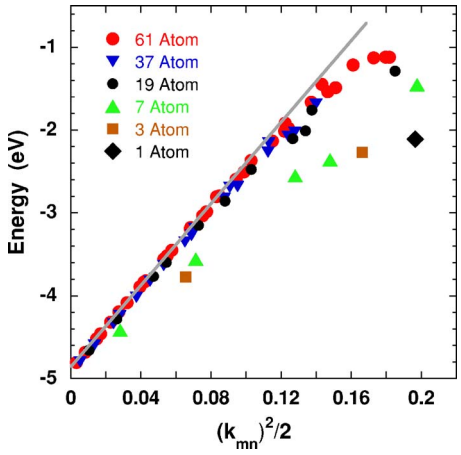


FIG. 9. (Color online) Energy of various $(m,n)$ quasistationary states for 1, 3, 7, 19, 37, and 61 Na atom nanoislands on Cu(111). The energy is referred to the vacuum level. The results are shown as a function of the quantized wave vector of the corresponding particle-in-a-box states (see the text for the definition). The different symbols represent states corresponding to the Na islands of different sizes, as shown in the inset. The solid line gives a linear fit to the energy according to $E_{mn}=E_{\mathrm{QW}}+k^2_{mn}/2$.

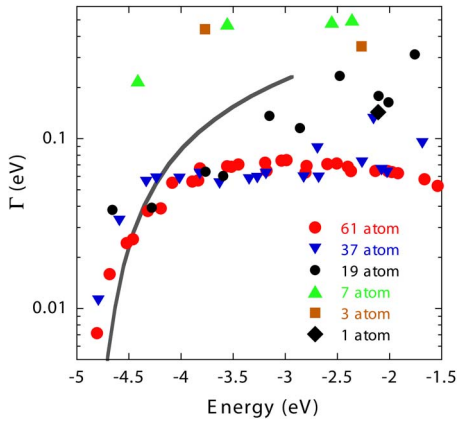


FIG. 10. (Color online) Widths of the various quasistationary $(m,n)$ states for the 1, 3, 7, 19, 37, and 61 Na atom islands on the Cu(111) surface. The widths are given as a function of the energy of the quasistationary state. The energy is referred to the vacuum level. The different symbols represent the states corresponding to the Na islands of different sizes, as shown in the inset. The solid line shows the many-body decay rate $\Gamma^{ee}(E)$ calculated for QWS's at 1 ML Na on the Cu(111) surface.

correctly predict the energies of the states in these islands, since it is based on the assumption of the perfect confinement of electron motion parallel to the surface inside the island. Similarly, for the large islands, increasing $(k_{mn})^2$ leads to the lowering of the binding energy of the state inside the potential well created by the nanoisland. The weight of the exponential tails of the wave functions outside the island boundary increases, and the energies drop from the particle-in-a-box line at large $(k_{mn})^2$; the earlier the drop the smaller the nanoisland.

It is noteworthy how fast the transition from the atomic-like excited state localized at a single adsorbate atom to QWS's confined to islands is. The states at the island as small as 7 Na atoms ($R_{\mathrm{Na}}=10.15$) already resemble the latter case. Extrapolating the present results to $R_{nm}/R_{\mathrm{Na}}=0$ we obtain $E_{\mathrm{QW}}=-4.9$ eV. The "asymptotic" QWS energy is thus 40 meV above the Fermi level of the model Cu(111) surface located at −4.94 eV. We recall that for the complete Na monolayer on the Cu(111) surface, the QWS energy is 127 meV below the Fermi level. Further calculations are necessary in order to find out if this difference is due to the fact that the present island sizes do not yet result in an accurate extrapolation. A second possibility is that the solution of our DFT calculation comprised of thousands of electrons is stuck before reaching the convergence at the level of accuracy required. Unfortunately, the present approach is computationally too demanding for larger islands.

The widths of the quasistationary states due to elastic one-electron tunneling are shown in Fig. 10. The results are not resolved in $m$, i.e., for the given island size, the states corresponding to different $m$ symmetries are represented by the same symbol. As a general observation, except for the 3 Na and 7 Na atom island cases, the widths of the quasistationary island-localized states are rather small, reflecting the stabilization of the states by the projected band gap. The stabilization effect is due to the fact that the resonant electron transfer into the substrate is impossible along the surface normal (see Figs. 5 and 7). Only substrate states with finite $k_{\parallel}$ can contribute to the excited state decay. Since the surface normal is the preferential direction for the resonant electron transfer, the transfer rates are reduced as compared, e.g., to free-electron metal substrates, where they typically reach the eV range.[15]

The results for the 3 Na island represent the transition from the single adsorbate to the particle-in-a-box case. For the larger islands the general trend in the dependence of the widths of the states on their energies can be established from Fig. 10: For the fixed island size, the most long-lived states are the ones with the lowest energies. This can be understood by adopting the particle-in-a-box picture where the QWS electron is moving inside the island and colliding with island boundaries. Scattering at the island boundaries leads to the quantization of the QWS continuum (formation of the discrete states), and to the decay due to the interband transitions to a 3D bulk or a 2D surface state. It follows from Eq. (12) that the lower the energy of the state $E_{mn}$, the smaller the corresponding electron momentum parallel to the surface $k_{mn}$. The island boundary acts as an infinite potential barrier for these slow electrons so that they are reflected back with a 100% efficiency, and no transitions into the substrate states are possible. When the energy of the quasistationary state grows, the electron momentum parallel to the surface increases and the island boundary becomes more and more transparent. The probability of transitions to substrate states increases as does the decay rate. Qualitatively the same results have been reported for electron states trapped inside quantum corrals,[32,56] as well as for surface states localized at Ag islands on the Ag(111) surface,[34] and for image states localized at Ar islands on the Cu(100) surface.[57] For states with low energies close to $E_{\mathrm{QW}}$, increasing the island size leads to an overall decrease of the widths of the states. One would expect this effect, recalling that for the limit of the infinite Na monolayer the discrete states should merge into the 2D continuum of the QWS with no one-electron decay possible.

Figure 10 shows that at high energies the one-electron widths for the largest islands saturate close to 60 meV. The saturation is due to two competing phenomena nearly canceling each other. As we have discussed above, the higher the energy of the state, the lower reflectivity of the island boundary so that the lifetime of the state decreases. On the other hand, as the energy of the island-localized state rises, it appears higher in the projected band gap of the Cu(111) surface. Obviously, substrate states accessible to the electron transfer are those with larger $k_{\parallel}$'s (see Fig. 7), so that the efficiency of the electron transfer decreases. In the 61 Na atom island case, there is even a slight decrease of the widths at high energies meaning that the latter effect, decrease of the phase space, starts to dominate.

Being a one-electron treatment, the WPP technique does not account for the inelastic energy relaxation of excited states due to many-body effects such as the electron-electron scattering. It has been shown previously, that the elastic resonant one-electron transfer and inelastic processes can be treated independently because they give additive contributions to the total decay rate $\Gamma_{mn}^{\mathrm{total}}$ of the population of an

excited state.[15] Thus, $\Gamma_{mn}^{\text{total}}=1/\tau_{mn}=\Gamma_{mn}+\Gamma_{mn}^{ee}$, where $\Gamma_{mn}^{ee}$ stands for the inelastic electron-electron interaction contribution to the decay and $\tau_{mn}$ is the lifetime of the excited state. Accurate calculation of $\Gamma_{mn}^{ee}$ for excited states in the island-localized states is not feasible at present because of the very time consuming computations of the response function.[7] Instead we estimate the upper limit $\Gamma_{mn}^{ee}$ from the corresponding decay rates of a QWS for the 1ML Na/Cu(111) surface taken at the energy $E_{mn}$: $\Gamma_{mn}^{ee}=\Gamma^{ee}(E_{mn})$. This should be a reasonable procedure, especially for large Na islands. Indeed, as follows from our results, island-localized states converge to the 2D QWS continuum as the island size increases. Since for the 2D QWS continuum the intraband transitions give a noticeable contribution to $\Gamma^{ee}(E)$, $\Gamma^{ee}(E_{mn})$ should give the upper limit for the inelastic decay of the island-localized states because of the discretization of the QWS continuum by the island boundaries.

In Fig. 10 the solid line shows the many-body decay rate of QWS's for the 1 ML Na/Cu(111) surface calculated in Ref. 38. According to our results for the largest islands (19, 37, and 61 Na atoms), the single-electron widths, denoted by markers, fall at energies $E_{mn}>-4.2$ eV below the solid line. Thus the lifetimes of these states are determined by the many-body decay processes. For states with lower energies, the many-body decay rates are smaller than the one-electron decay rates for all the island sizes considered here. The one-electron decay rates are seen to decrease with the increasing island size, and we estimate that the inelastic electron-electron processes will completely dominate the decay of the island-localized states for islands with $R_{\text{Na}}\gtrsim 200$.

Finally, we estimate the maximum island size for which discrete resonance states can be resolved in experiments. The best resolution can be obtained by measuring, e.g., electron photoemission along the surface normal, or the density of states at the center of the island as accessible with scanning tunneling spectroscopy. In this geometry only the states with the $m=0$ symmetry will contribute to the signal. Neighboring states can be resolved when their energy difference is larger than one half of the sum of their widths. From this criteria we estimate that resonance states can still be resolved for islands consisting of several hundreds of atoms. This simple estimate does not take into account the additional broadening due to the variation of island sizes or due to defect or phonon scattering processes.

## IV. CONCLUSIONS

We have presented a systematic study of excited electron states localized by one-layer high Na nanoislands on the Cu(111) surface. The density functional formalism has been used to obtain electronic properties of the nanoislands such as the electron density and potential induced by adsorbed nanoislands. A one-dimensional pseudopotential for the Cu(111) substrate has been used along with the cylindrical jellium model for Na. The density functional calculations provide the input for a wave packet propagation study of the energies and lifetimes of quasistationary states (resonances) localized at Na islands. The Na/Cu(111) prototype system has been chosen because the single-adatom and the complete one-monolayer limits are well documented in the literature. We believe that the results obtained in the present study will deepen the general understanding of properties of electronic states localized at supported metallic nanoislands.

Our main results can be summarized as follows.

(1) For islands consisting of 19 or more Na atoms, the calculated resonance states correspond nicely to the particle-in-a-box picture of 1ML Na/Cu(111) with the quantum well state trapped inside the island. For the 1ML Na/Cu(111) surface the quantum well state is stable against one-electron decay. However, for finite size Na islands, the scattering of the QWS electron at the island boundaries leads to (i) the quantization of the 2D QWS continuum so that discrete states emerge; to (ii) the possibility of the energy-conserving resonant one-electron transfer into the 3D continuum of the bulk states or into the 2D continuum of the surface state of Cu(111). Thus, the discrete island-localized states are broadened into the resonances, i.e., they become quasistationary.

(2) On the basis of the calculated energies and widths of the quasistationary states, it appears that the transition from the atomic-like state localized at a single Na adsorbate atom to the particle-in-a-box picture is very fast as the island size increases. The intermediate regime is limited to islands of three and seven Na atoms in our calculations. For larger islands, the calculated energies of the quasistationary states are well described by the simple model assuming perfect electron trapping inside the island.

(3) The island-localized states appear quite stable with respect to the one-electron decay into the substrate. This is entirely due to the projected band gap of Cu(111) (the so-called band gap stabilization effect).

(4) The one-electron decay rate of the states decreases in overall with the increasing island size, which simply reflects that the states converge toward the 2D quantum well states. For the fixed island size, the one-electron decay drops exponentially for the low energy states corresponding to the slow electron motion parallel to the surface. This is because the island boundary becomes perfectly reflective. As the energy rises, the reflectivity of the island boundary decreases and the decay rate increases. However, this is counterbalanced by the band-gap stabilization effect which is more efficient for higher energy states. Thus, the widths of the states tend to level off.

(5) The comparison of the relative efficiencies of the one-electron (elastic) and many-body (inelastic) decays shows that for small islands the resonant electron transfer into the substrate is the main decay channel for the island-localized states. For the largest islands considered here (37 and 61 Na atoms) the lifetimes of the quasistationary states with energies $E_{mn}>-4.2$ eV are determined by the many-body decay processes. At lower energies the one-electron decay is more important. Islands comprised of the order of 200 Na atoms are needed for the many-body processes to be the main decay channel.

(6) Finally, the results of the present study show how the 2D continuum of the surface-localized state is perturbed by finite-size effects in a direction parallel to the surface. In the present study the 2D continuum is that of a quantum well state due to the adsorbate. However, this system has a direct link with the quantization of the 2D clean surface state con-

tinuum observed, e.g., for quantum corrals[32,33] and for Ag addatom[27] or vacancy[34] islands on the Ag(111) surface. Indeed, the present results and conclusions are very much in line with the results of these studies.

## ACKNOWLEDGMENTS

We acknowledge the partial support from the Academy of Finland through its Centers of Excellence project, the Finnish Funding Agency for Technology and Innovation (TEKES), the Finnish IT center CSC, the University of the Basque Country UPV/EHU (Grant No. 9/UPV 00206.215-13639/2001), the Departamento de Educación, Universidades e Investigatión del Gobierno Vasco, the Spanish Ministerio de Ciencia y Tecnología MCyT (Grant No. FIS2004-06490-C03-01), and the European Community 6th Network of Excellence NANOQUANTA (Grant No. NMP4-CT-2004-500198). Finally, M.J.P. thanks the Donostia International Physics Center for the warm hospitality during the sabbatical leave.

[1] Th. Fauster and W. Steinmann, In *Photonic Probes of Surfaces*, Vol. 2 of *Electromagnetic Waves: Recent Developments in Research*, edited by P. Halevi (North-Holland, Amsterdam, The Netherlands, 1995), Chap. 8, p. 347.
[2] H. Petek and S. Ogawa, Prog. Surf. Sci. **56**, 239 (1997).
[3] U. Höfer, I. L. Shumay, Ch. Reuss, U. Thomann, W. Wallauer, and Th. Fauster, Science **277**, 1480 (1997).
[4] R. Matzdorf, Surf. Sci. Rep. **30**, 153 (1998); E. V. Chulkov, I. Sarría, V. M. Silkin, J. M. Pitarke, and P. M. Echenique, Phys. Rev. Lett. **80**, 4947 (1998).
[5] J. Kliewer, R. Berndt, E. V. Chulkov, V. M. Silkin, P. M. Echenique, and S. Crampin, Science **288**, 1399 (2000).
[6] M. Weinelt, J. Phys.: Condens. Matter **14**, R1099 (2002).
[7] P. M. Echenique, R. Berndt, E. V. Chulkov, Th. Fauster, A. Goldmann, and U. Höfer, Surf. Sci. Rep. **52**, 219 (2004).
[8] J. Kröger, L. Limot, H. Jensen, R. Berndt, S. Crampin, and E. Pehlke, Prog. Surf. Sci. **80**, 26 (2005); J. Güdde and U. Höfer, *ibid.* **80**, 49 (2005); E. V. Chulkov, A. G. Borisov, J. P. Gauyacq, D. Sanchez-Portal, V. M. Silkin, V. P. Zhukov, and P. M. Echenique, Chem. Rev. (Washington, D.C.) **106**, 4160 (2006); Ph. Hofmann, Prog. Surf. Sci. **81**, 191 (2006); J. Güdde, W. Berthold, and U. Höfer, Chem. Rev. (Washington, D.C.) **106**, 4261 (2006); C. D. Lindstrom and X.-Y. Zhu, *ibid.* **106**, 4281 (2006).
[9] X.-Y. Zhu, J. Phys. Chem. B **108**, 8778 (2004).
[10] P. Avouris and R. E. Walkup, Annu. Rev. Phys. Chem. **40**, 173 (1989); C. Frischkorn and M. Wolf, Chem. Rev. (Washington, D.C.) **106**, 4207 (2006).
[11] E. Knoesel, A. Hotzel, and M. Wolf, Phys. Rev. B **57**, 12812 (1998).
[12] L. Bürgi, O. Jeandupeux, H. Brune, and K. Kern, Phys. Rev. Lett. **82**, 4516 (1999); K.-F. Braun and K.-H. Rieder, *ibid.* **88**, 096801 (2002).
[13] M. Bauer, S. Pawlik, and M. Aeschlimann, Phys. Rev. B **55**, 10040 (1997); M. Bauer, S. Pawlik, and M. Aeschlimann, *ibid.* **60**, 5016 (1999); S. Ogawa, H. Nagano, and H. Petek, Phys. Rev. Lett. **82**, 1931 (1999); H. Petek, M. J. Weid, H. Nagano, and S. Ogawa, Science **288**, 1402 (2000); H. Petek, H. Nagano, M. J. Weida, and S. Ogawa, J. Phys. Chem. B **105**, 6767 (2001).
[14] A. G. Borisov, A. K. Kazansky, and J. P. Gauyacq, Surf. Sci. **430**, 165 (1999).
[15] A. G. Borisov, J. P. Gauyacq, A. K. Kazansky, E. V. Chulkov, V. M. Silkin, and P. M. Echenique, Phys. Rev. Lett. **86**, 488 (2001); A. G. Borisov, J. P. Gauyacq, E. V. Chulkov, V. M. Silkin, and P. M. Echenique, Phys. Rev. B **65**, 235434 (2002).
[16] S. Å. Lindgren and L. Walldén, Phys. Rev. Lett. **59**, 3003 (1987); Phys. Rev. B **38**, 3060 (1988); R. Dudde, L. S. O. Johansson, and B. Reihl, *ibid.* **44**, 1198 (1991); N. Fischer, S. Schuppler, R. Fischer, Th. Fauster, and W. Steinmann, *ibid.* **43**, 14722 (1991).
[17] A. Carlsson, S.-Å. Lindgren, C. Svensson, and L. Walldén, Phys. Rev. B **50**, 8926 (1994).
[18] N. Fischer, S. Schuppler, Th. Fauster, and W. Steinmann, Surf. Sci. **314**, 89 (1994).
[19] A. Carlsson, B. Hellsing, S.-Å. Lindgren, and L. Walldén, Phys. Rev. B **56**, 1593 (1997).
[20] J. Kliewer and R. Berndt, Surf. Sci. **477**, 250 (2001).
[21] J. Kliewer and R. Berndt, Phys. Rev. B **65**, 035412 (2001).
[22] J. M. Carlsson and B. Hellsing, Phys. Rev. B **61**, 13973 (2000).
[23] E. V. Chulkov, J. Kliewer, R. Berndt, V. M. Silkin, B. Hellsing, S. Crampin, and P. M. Echenique, Phys. Rev. B **68**, 195422 (2003).
[24] T. Miller, A. Samsavar, G. E. Franklin, and T. -C. Chiang, Phys. Rev. Lett. **61**, 1404 (1988); J. J. Paggel, T. Miller, T. C. Chiang, Science **283**, 1709 (1999); T. C. Chiang, Surf. Sci. Rep. **39**, 181 (2000); E. V. Chulkov and V. M. Silkin, Surf. Sci. **215**, 385 (1989).
[25] F. J. Himpsel, J. E. Ortega, G. J. Mankey, and R. F. Willis, Adv. Phys. **47**, 511 (1998); M. Milun, P. Pervan, and D. P. Woodruff, Rep. Prog. Phys. **65**, 99 (2002); E. Ogando, N. Zabala, E. V. Chulkov, and M. J. Puska, Phys. Rev. B **69**, 153410 (2004); C. Koitzsch, C. Battaglia, F. Clerc, L. Despont, M. G. Garnier, and P. Aebi, Phys. Rev. Lett. **95**, 126401 (2005); F. Schiller, R. Keyling, E. V. Chulkov, and J. E. Ortega, *ibid.* **95**, 126402 (2005); S. Mathias, M. Wiesenmayer, M. Aeschlimann, and M. Bauer, *ibid.* **97**, 236809 (2006).
[26] H. Roder, E. Hahn, H. Brune, J.-P. Bucher, and K. Kern, Nature (London) **366**, 141 (1993).
[27] J. Li, W. D. Schneider, R. Berndt, and S. Crampin, Phys. Rev. Lett. **80**, 3332 (1998).
[28] R. D. Diehl and R. McGrath, Surf. Sci. Rep. **23**, 43 (1996).
[29] C. T. Campbell, Surf. Sci. Rep. **27**, 1 (1997).
[30] M. Valden, X. Lai, and D. W. Goodman, Science **281**, 1647 (1998).
[31] T. Torsti, V. Lindberg, M. J. Puska, and B. Hellsing, Phys. Rev. B **66**, 235420 (2002); V. Lindberg, and B. Hellsing, J. Phys.: Condens. Matter **17**, S1075 (2005); V. Lindberg, T. Petersson, and B. Hellsing, Surf. Sci. **600**, 6 (2006).
[32] E. J. Heller, M. F. Crommie, C. P. Lutz, and D. M. Eigler, Nature (London) **369**, 464 (1994).
[33] H. C. Manoharan, C. P. Lutz, and D. M. Eigler, Nature (London) **403**, 512 (2000).

[34] H. Jensen, J. Kröger, R. Berndt, and S. Crampin, Phys. Rev. B **71**, 155417 (2005).
[35] For a recent review, see *A Primer in Density Functional Theory, Lecture Notes in Physics*, edited by C. Fiolhais, F. Nogueira, and M. Marques, No. 620, (Springer, Berlin, 2003).
[36] E. Ogando, N. Zabala, E. V. Chulkov, and M. J. Puska, Phys. Rev. B **71**, 205401 (2005).
[37] E. V. Chulkov, V. M. Silkin, and P. M. Echenique, Surf. Sci. **437**, 330 (1999).
[38] V. M. Silkin, M. Quijada, R. Díez Muiño, E. V. Chulkov, and P. M. Echenique (unpublished).
[39] We use the exchange-correlation functionals based on the quantum Monte Carlo calculations by D. M. Ceperley and B. J. Alder, Phys. Rev. Lett. **45**, 566 (1980) and parametrized by J. P. Perdew and A. Zunger, Phys. Rev. B **23**, 5048 (1981).
[40] M. Heiskanen, T. Torsti, M. J. Puska, and R. M. Nieminen, Phys. Rev. B **63**, 245106 (2001).
[41] T. Torsti, V. Lindberg, M. J. Puska, and B. Hellsing, Phys. Rev. B **66**, 235420 (2002).
[42] V. S. Stepanyuk, D. I. Bazhanov, A. N. Baranov, W. Hergert, P. H. Dederichs, and J. Kirschner, Phys. Rev. B **62**, 15398 (2000).
[43] C. Kittel, *Introduction to Solid State Physics*, 7th ed. (Wiley, New York, 1996), pp. 248–252.
[44] A. G. Borisov, J. P. Gauyacq, and S. V. Shabanov, Surf. Sci. **487**, 243 (2001).
[45] A. G. Borisov, A. K. Kazansky, and J. P. Gauyacq, Phys. Rev. B **59**, 10935 (1999)
[46] F. E. Olsson, A. G. Borisov, and J. P. Gauyacq, Surf. Sci. **600**, 2184 (2006).
[47] D. Neuhauser and M. Baer, J. Chem. Phys. **91**, 4651 (1989).
[48] M. D. Feit, J. A. Fleck, Jr., and A. Steiger, J. Comput. Phys. **47**, 412 (1982).
[49] R. Kosloff, J. Phys. Chem. **92**, 2087 (1988).
[50] J. R. Taylor, *Scattering Theory: The Quantum Theory of Nonrelativistic Collisions* (Krieger, Malabar, FL, 1983).
[51] M. R. Wall and J. Neuhauser, J. Chem. Phys. **102**, 8011 (1995).
[52] V. A. Mandelshtam and H. S. Taylor, Phys. Rev. Lett. **78**, 3274 (1997).
[53] D. Neuhauser, J. Chem. Phys. **93**, 2611 (1990).
[54] C. Corriol, V. M. Silkin, D. Sánchez-Portal, A. Arnau, E. V. Chulkov, P. M. Echenique, T. von Hofe, J. Kliewer, J. Kröger, and R. Berndt, Phys. Rev. Lett. **95**, 176802 (2005).
[55] A. G. Borisov, A. K. Kazansky, and J. P. Gauyacq, Phys. Rev. B **65**, 205414 (2002).
[56] L. Niebergall, G. Rodary, H. F. Ding, D. Sander, V. S. Stepanyuk, P. Bruno, and J. Kirschner, Phys. Rev. B **74**, 195436 (2006).
[57] J. P. Gauyacq and A. G. Borisov, Surf. Sci. **600**, 825 (2006).